Research in Particle Physics

2+1 flavor QCD at Physical Point on very large lattices (master-field simulations)

Hadrons are the constituents of atomic nuclei. Computing the mass spectrum of hadrons from first principles of the quantum chromodynamics (QCD), the fundamental theory of strong interaction described by quarks and gluons, is a principal subject in particle physics.

After quenched and succeeding 2 flavor QCD simulations by the CP-PACS, those studies were extended to 2+1 flavor QCD by incorporating the dynamical strange quark, though the degenerate up-down quark mass was much heavier than the physical one. On the PACS-CS and the T2K computers, we have succeeded in reaching the physical point. This calculation is followed by a larger volume simulation on the K computer.

Our current project is aiming to control and remove systematic errors due to the previous simulations on a finite volume with a finite lattice spacing. We are performing so called master-field simulations on very larger $(10\text{fm})^4$ volume with several lattice spacings using the Oakforest-PACS.

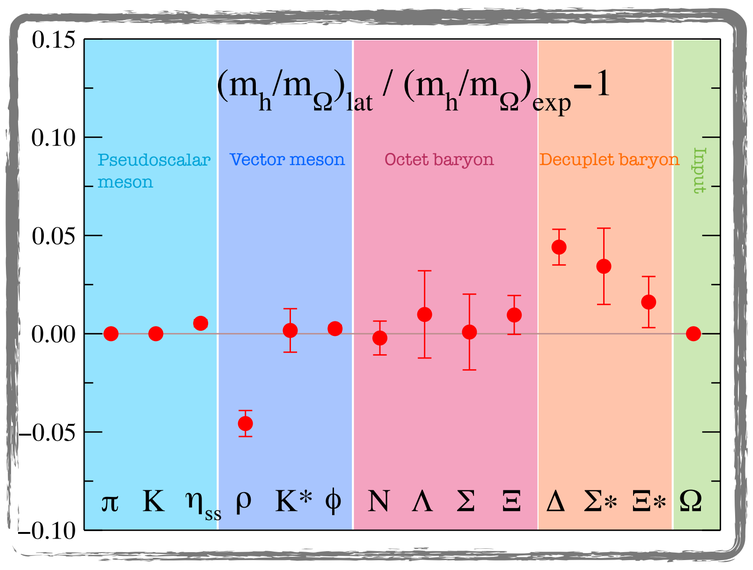

Fig1a:
Relative difference of the light hadron spectrum from the experiment. Inputs are only the pion, kaon, and omega baryon masses to determine the up-down and strange quark masses, and the lattice cutoff, respectively. Our results show good agreement with the experiment albeit errors are still not quite small for some of the hadrons.
[K-.I. Ishikawa et al., https://arxiv.org/abs/1511.09222]

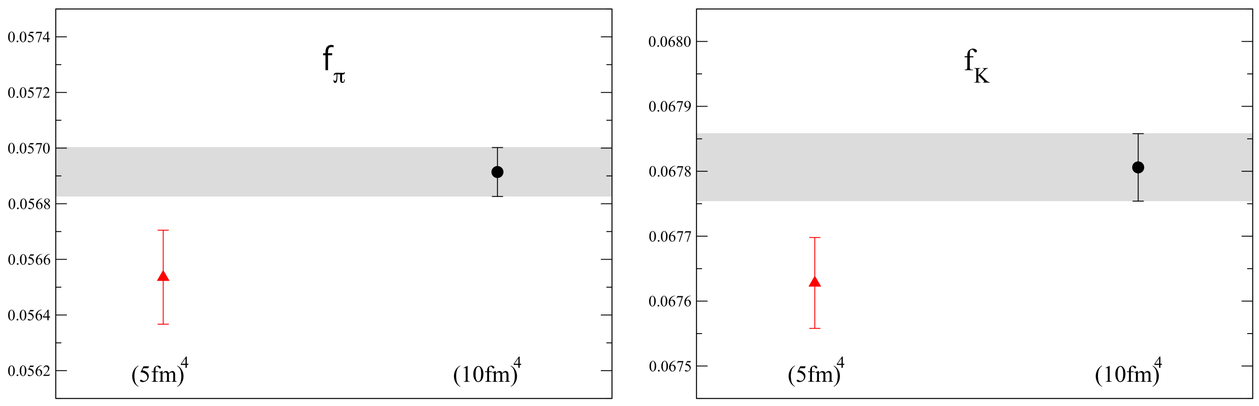

Fig. 1b:
A comparison of pseudoscalar decay constants, f_π and f_K, on $(10\text{fm})^4$ and $(5\text{fm})^4$. We detect 0.66% and 0.26% finite volume effect on f_π and f_K, respectively. The effect is very small and negligible to compare the corresponding experiments. Now, we can control and remove the finite volume effect completely by using the master-field simulations.
[K-.I. Ishikawa et al., Phys. Rev. D 99, 014504]

Exploring QCD phase diagram

Investigating the phase structure of QCD at non-zero temperature and density is very important to understand properties of strongly interacting matters under extreme conditions. It is known that the order of the phase transition depends on the mass and the number of flavors of quarks and there should be so-called critical endlines, lines of second order phase transitions, in certain space of quark masses as shown in Fig. 2a.

To determine the shape of the critical endline in the small quark mass region we are carrying out lattice QCD simulations at finite temperature with 2+1 as well as 3 degenerate quark flavors on Cygnus and Oakforest-PACS. Fig. 2b shows our recent estimation of the critical pion mass in 3 flavor QCD in the continuum limit including a new calculation with the temporal lattice extent of 12, where the new result gives a smaller upper bound than that of our previous calculation.

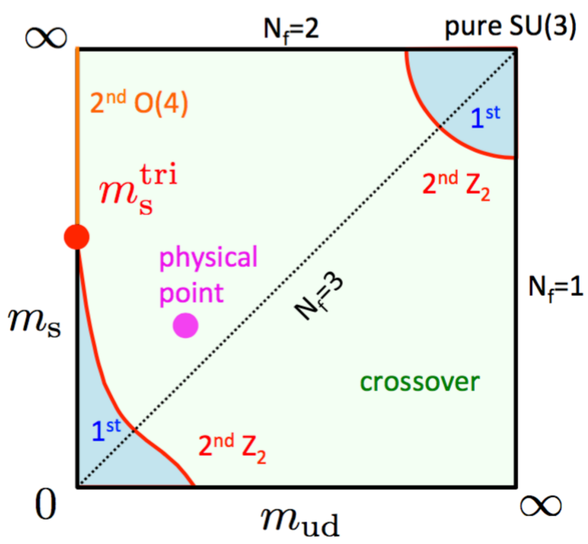

Fig. 2a:
Expected quark mass dependence of the order of the QCD phase transition. Our goal is to determine the shape of the critical endline shown as a red curve in the lower-left corner.

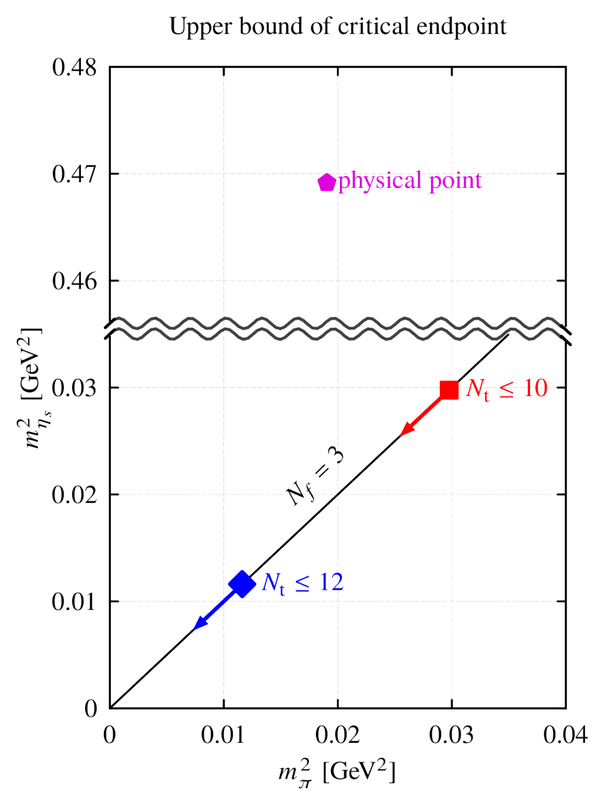

Fig. 2b:
Our recent estimation of the critical pion mass, $m_{\pi,E}$, in 3 flavor QCD. The continuum extrapolation including new data sets with the temporal extent of 12 gives an upper bound $m_{\pi,E} \lesssim 110$ MeV.
[Y. Kuramashi et al., Phys. Rev. D 101, 054509]

Solving the Mysteries of the Universe with Computational Astrophysics

Vlasov-Poisson simulation of cosmic neutrinos in the large-scale structure of the universe

Neutrinos are elementary particles ubiquitous in the universe. The Super-Kamiokande experiment revealed that neutrinos have mass, which implies that neutrinos can dynamically affect the formation of large-scale structure (LSS) in the universe. We perform numerical simulations of LSS formation incorporating the effect of massive neutrinos by directly solving the collisionless Boltzmann equation in 6D phase-space on two supercomputers, FUGAKU and Oakforest-PACS. Our highly optimized simulation code achieves almost ideal weak and strong scaling on FUGAKU.

Yoshikawa, K., Tanaka, S., Yoshida, N. & Saito, S. (2020) accepted for publication in ApJ.

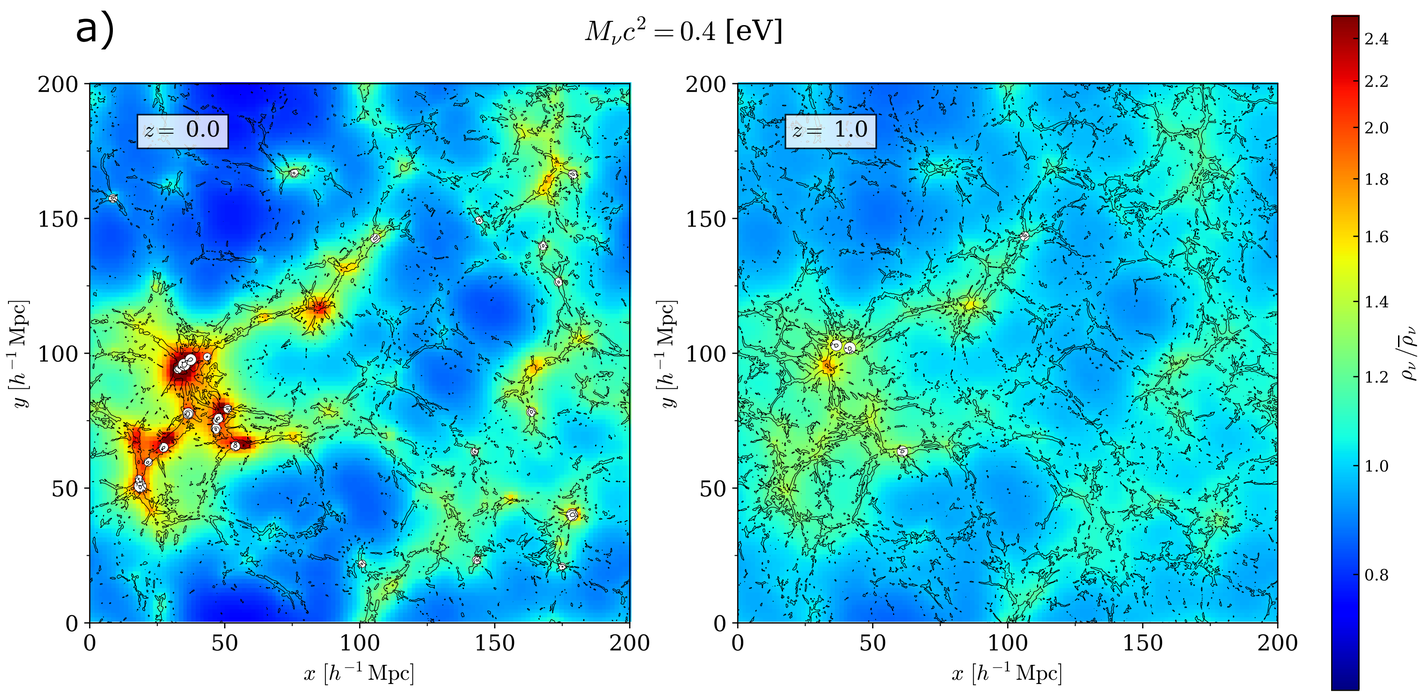

Fig. 1a: Simulated distributions of massive neutrinos (color scale) and dark matter (contours) as well as dark matter halos (white circle) at a) redshift z = 0 (the present), and b) redshift of 1 (about 7.9 Gyr ago).

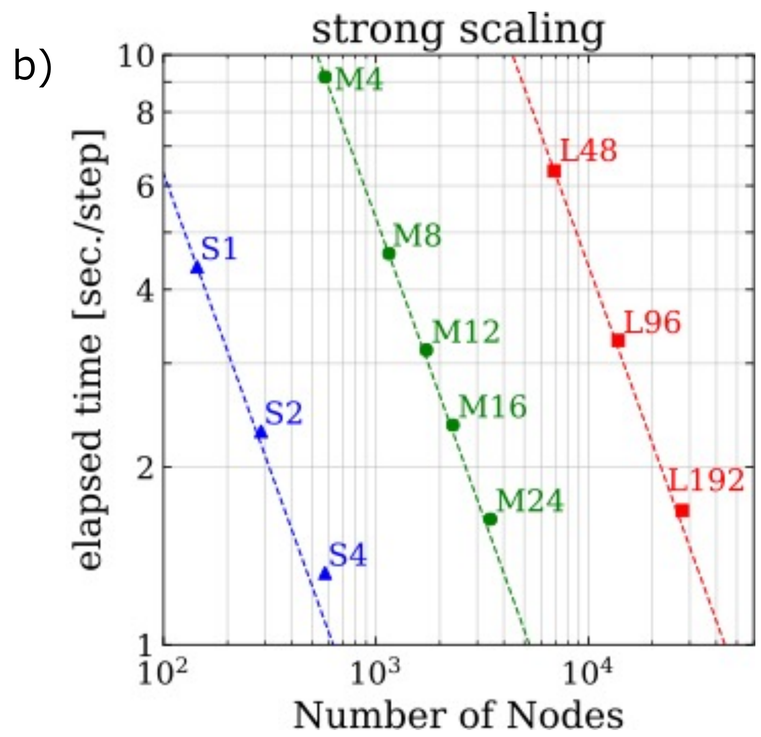

Fig. 1b: Strong scaling of VLASOV simulations on super computer FUGAKU. Run ID prefixes S, M, and L denote grid resolutions of 96^3, 192^3, and 384^3, respectively, and the number denotes the number of computational nodes in multiples of 144.

Theoretical galaxy formation – numerical simulations reveal the fate of stars and gas

We devise a physical model to determine the formation, distribution, and kinematics of molecular gas clouds in galaxies, and predict the intensities of carbon monoxide (CO) lines and the molecular hydrogen (H_2) abundance, taking into account the interstellar radiation field and dust attenuation. We apply the model to data from the Illustris-TNG cosmological simulations and compare the CO luminosities and H_2 masses with recent observations of galaxies at low and high redshifts. The model successfully reproduces the observed CO-luminosity function and the total H_2 mass in the local universe.

Inoue, S., Yoshida, N. & Yajima, H., (2020) accepted for publication in MNRAS

When a cluster of stars forms, only a part of the natal cloud is converted into stars, and the rest is ionized and heated by the powerful stellar radiation and ejected outward. Using radiation-hydrodynamic simulations, we found that star formation is primarily controlled by the formation of ionized regions, as well as the surface density and dust content of the natal cloud. We developed a new semi-analytic model that captures this behaviour and can be incorporated in subgrid recipes for large-scale cosmological simulations.

Fukushima, Yajima, et al. (2020), MNRAS, 497, 3830

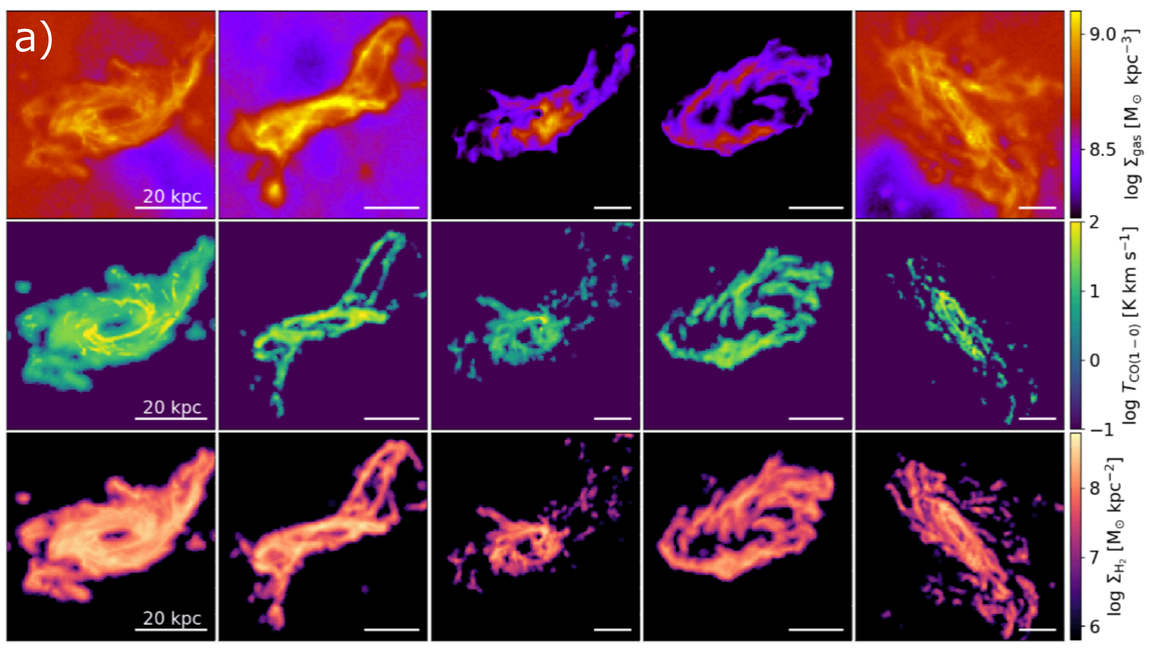

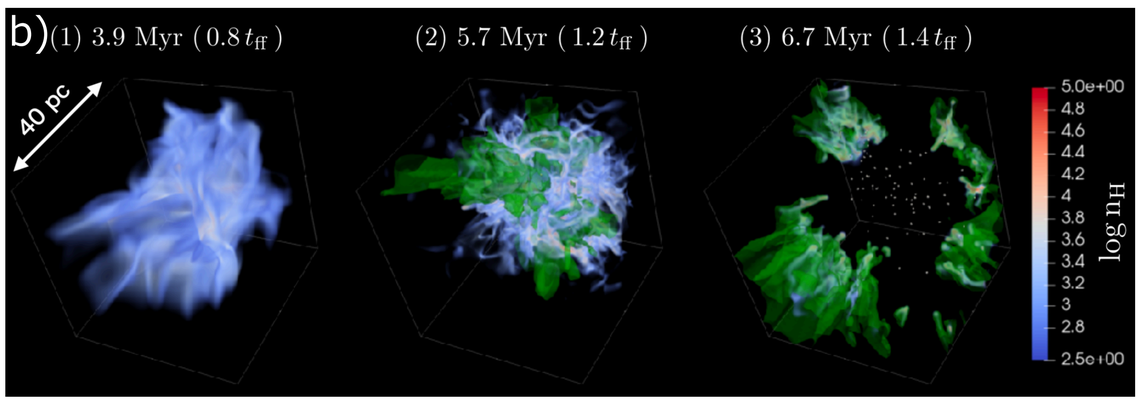

Fig. 2a: The structure of the five brightest galaxies in CO(1-0) in the simulation.
Fig. 2b: Density evolution in the formation of star clusters. White circles indicate stars and the green contours bound ionization regions.

contact address: ayw@ccs.tsukuba.ac.jp / pr@ccs.tsukuba.ac.jp

Computational Nuclear Physics

Are “free neutrons” in neutron stars free?

Although the nucleus is a microscopic object on earth, there is a gigantic nucleus in the universe, that is the neutron star (Fig.1). Near the surface of the neutron stars, a periodic crystalline structure is formed and all the protons are expected to be confined. In contrast, there are unbound neutrons which are regarded as “free”. These free neutrons play a key role in various observed phenomena, such as pulsar glitch and cooling.

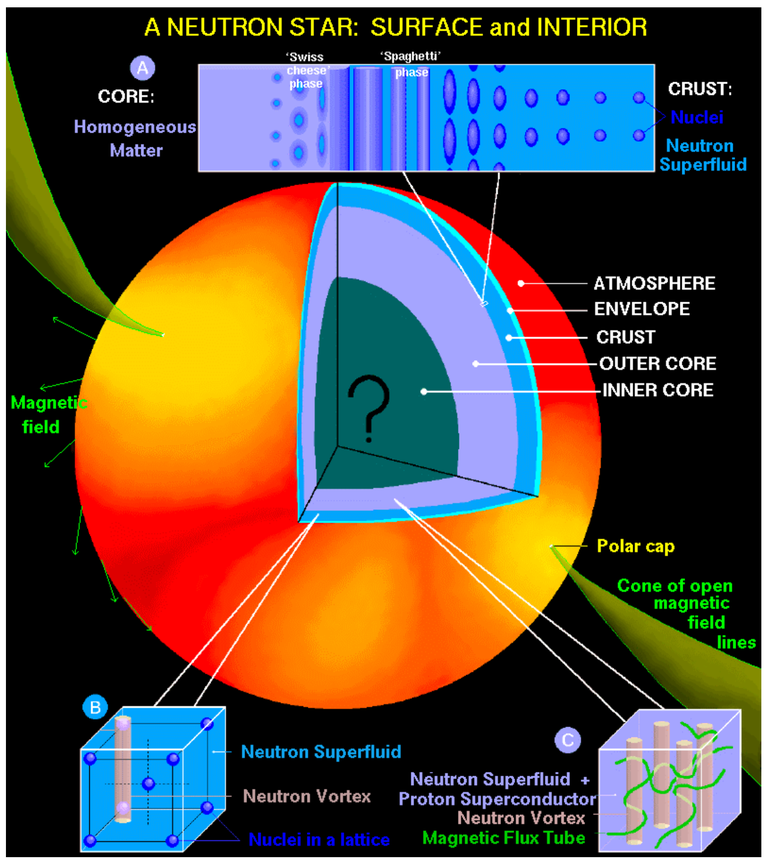

Fig. 1: Structure of a neutron star
Courtesy of http://www.astroscu.unam.mx/neutrones/

We have examined properties of the “free neutrons”, with the nuclear density functional calculation. Surprisingly, at a certain density region, they are even “super-free”, which means that their mass is lighter in the neutron star than in the vacuum (Fig.2)!

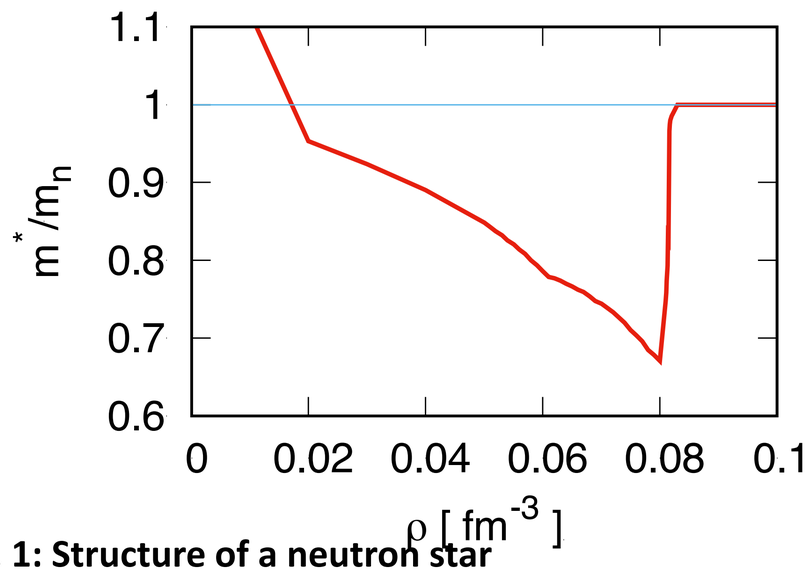

Fig. 2: Ratio of effective mass of free neutrons in the neutron-star crust (slab phase) to their bare mass.

Interactive Plot of Atomic nuclei and Computed Shapes (InPACS)

Measuring nuclear properties is very expensive using accelerators. The obtained data are precious for various technologies of human beings, thus, compiled by nuclear data centers in the world, then, open to public. We have calculated almost all kinds of nuclides in the universe, using the energy density functional theory. The computation complements missing experimental data. In order to publicize the computational nuclear data, we have opened a web site, InPACS, in which you may interactively obtain various nuclear data/information.

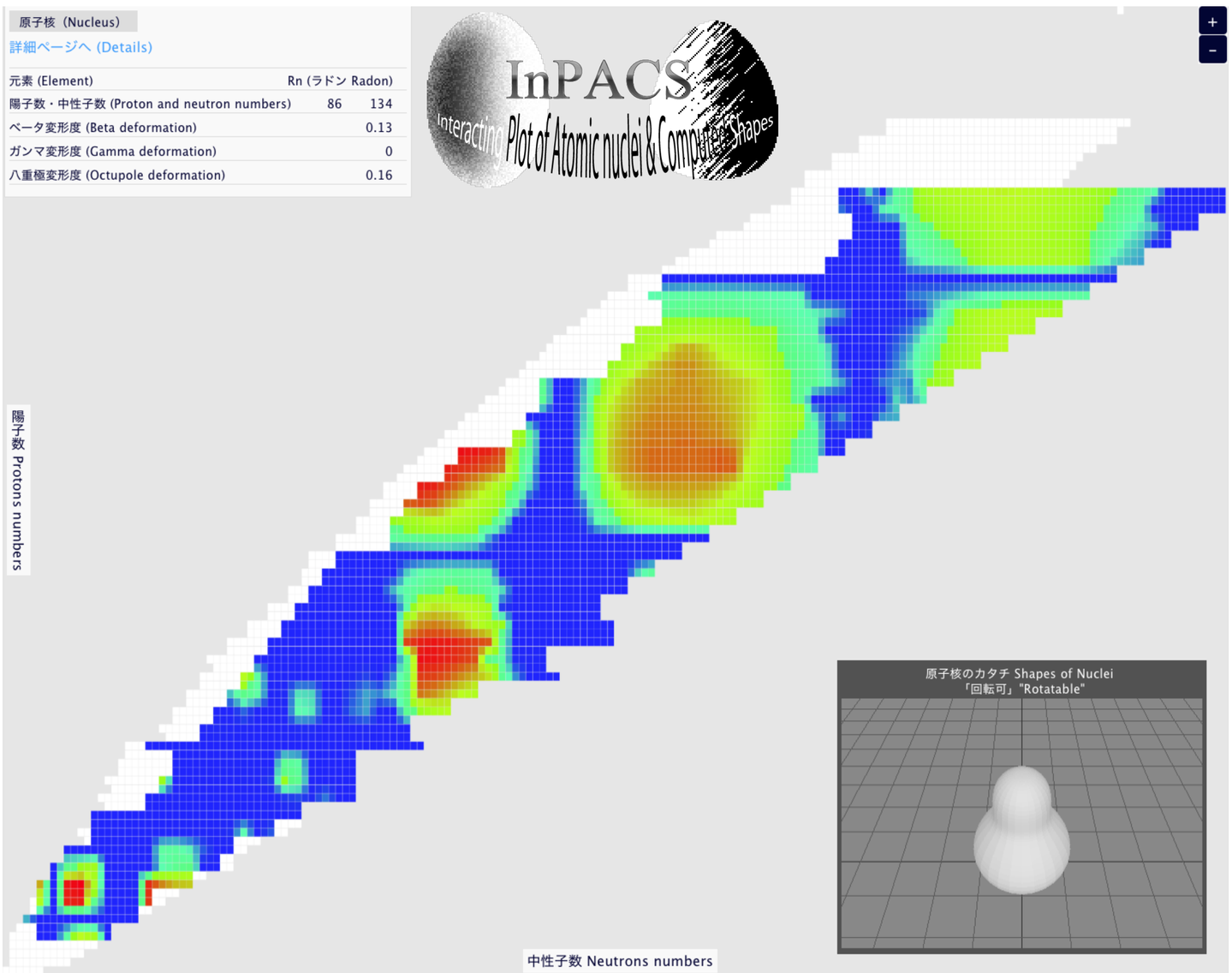

Fig. 3: Snapshot of InPACS web site.

This research was supported by ImPACT project on Reduction and Resource Recycling of High-level Radioactive Wastes through Nuclear Transmutation.

contact address: nakatsukasa@nucl.ph.tsukuba.ac.jp

Quantum Condensed Matter Physics

SALMON: Scalable Ab-initio Light-Matter simulator for Optics and Nanoscience

Understanding interaction between light and matter is the basis of a wide range of technologies. For this purpose, it is essential to describe electron dynamics in matters induced by light electromagnetic fields in a microscopic scale, 10^{-9} (nano-)meter in space and 10^{-15} (femto-) second in time. We have been developing an open-source computer code SALMON, Scalable Ab-initio Light-Matter simulator for Optics and Nanoscience that describes electron dynamics in molecules, nano-materials, and solids based on first-principles time-dependent density functional theory [http://salmon-tddft.jp]. As a novel function of SALMON, light propagation in nano-materials as well as in bulk medium can be described taking full account of nonlinearity and nonlocality of light-matter interactions in the ab-initio level. We expect SALMON will be widely used in cutting-edge researches in optics and nanoscience.

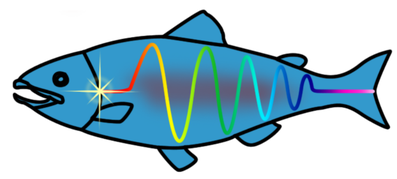

(a)

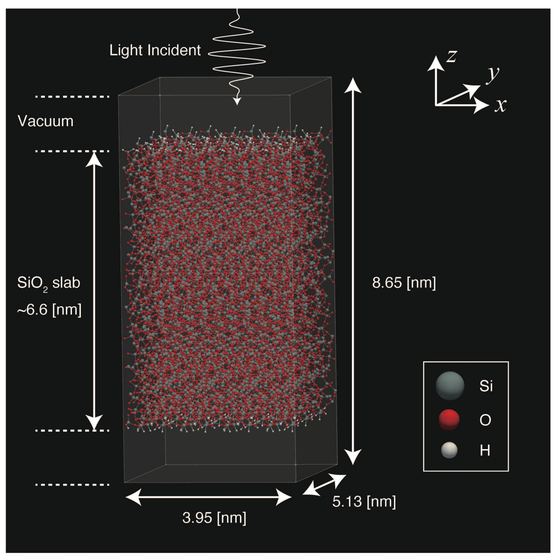

(a) A multiphysics simulation solving Maxwell, time-dependent Kohn-Sham, and Newton equations is performed on the Fugaku system for a thin film of amorphous SiO_2 composed of more than 10,000 atoms.

(b)

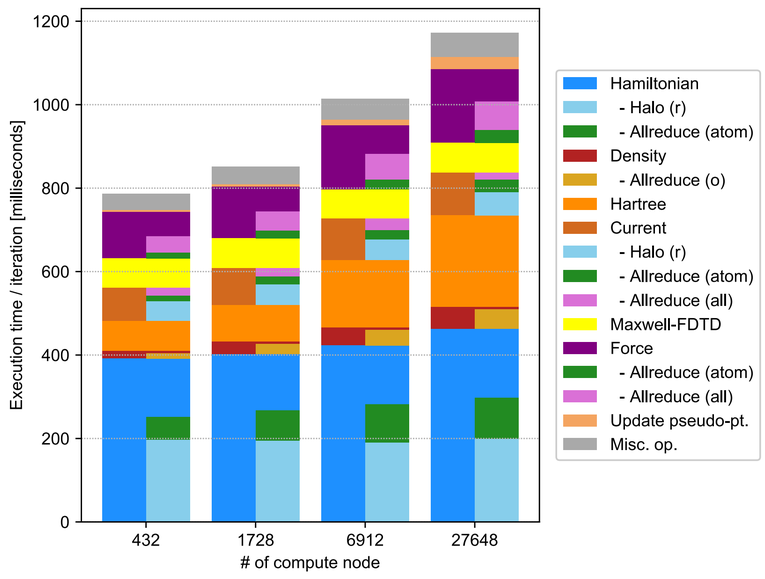

(b) Weak-scaling performance on the Fugaku system using up to 27,648 nodes to simulate 13,648 atoms.

Disclaimer

The results obtained on the evaluation environment in the trial phase do not guarantee the performance, power and other attributes of the supercomputer Fugaku at the start of its public use operation.

Optical Properties of Nano-materials in Real Time and Real Space

(a) Optical near-field generated in metal-organic framework, IRMOF-10

When a light pulse irradiates on nano-sized objects, a strong and spatially-localized electromagnetic field, which is called the near field, appears around the object. The near field enables imaging beyond the limit of optical resolution and enhances nonlinear optical processes. We perform first-principles calculations of the photoexcitation dynamics of an acetylene molecule in a metal organic framework, IRMOF-10. Resonant laser excitation of the IRMOF-10 generates an optical near field around the two benzene rings that comprise the main framework of the IRMOF-10. The second harmonic excitation caused by spatial nonuniformity of the optical near field is observed.

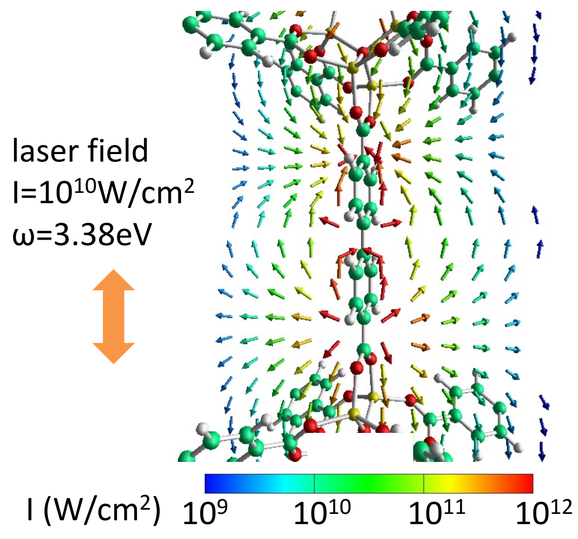

(b) Optical property of metallic metasurface with sub-nm gaps

By virtue of rapid progresses in fabrications of nano-materials, it is possible to manufacture periodic materials composed of uniformly structured nano-objects. Here we investigate the optical properties of quantum plasmonic metasurfaces composed of two-dimensional arrayed metallic nano-spheres with sub-nm gaps according to the time-dependent density functional theory, a fully quantum mechanical approach. When the quantum and classical descriptions are compared, the absorption rates of the metasurface exhibit substantial differences at shorter gap distances. The differences are caused by electron transport through the gaps of the nano-objects.

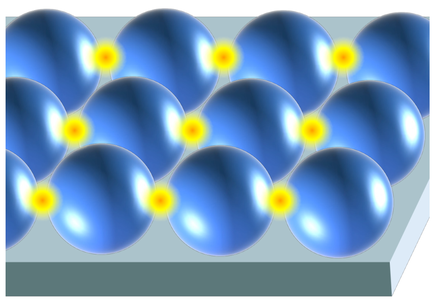

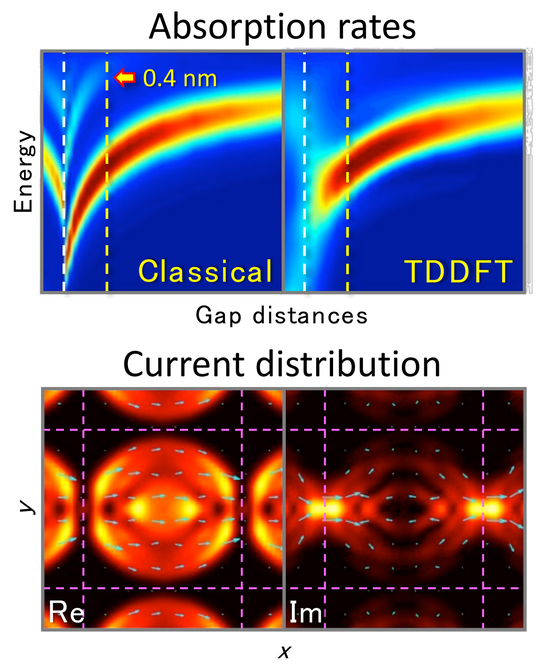

Computational Elucidations for Biomolecules

GPU-accelerated Molecular Orbital Calculation

Large-scale *ab initio* molecular orbital calculation is a target application in quantum chemistry for HPC computer systems, and the fragment molecular orbital (FMO) method is one of such application because it is designed for parallel computer. We have developed GPU-accelerated FMO calculation program with CUDA, and obtained 3.8x speedups from CPU on-the-fly FMO calculation of 1,961 atomic protein. [H. Umeda et al., IPSJ Transactions on Advanced Computing Systems 6, 4, (2013) 26-37. H. Umeda et al., SC15 poster (2015).]

(a)

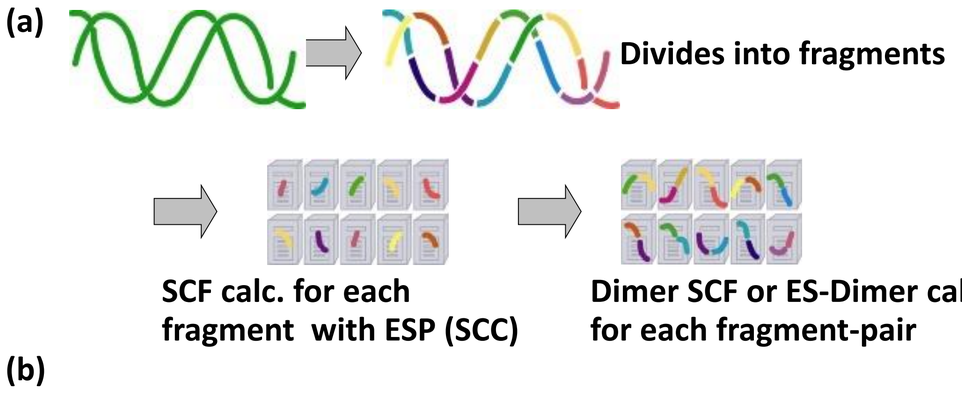

(b)

Application	Lysozyme			HA3
#Atoms	1,961			23,460
#Nodes (#GPU)	8 (0)	8 (32)		64 (256)
SCC	3,071 s	828 s	3.7x	0.52 hr
Dimer SCF	6,246 s	1,675 s	3.7x	0.90 hr
ES Dimer	407 s	78 s	5.2x	0.45 hr
Total	9,770 s	2,597 s	3.8x	1.97 hr

(c)

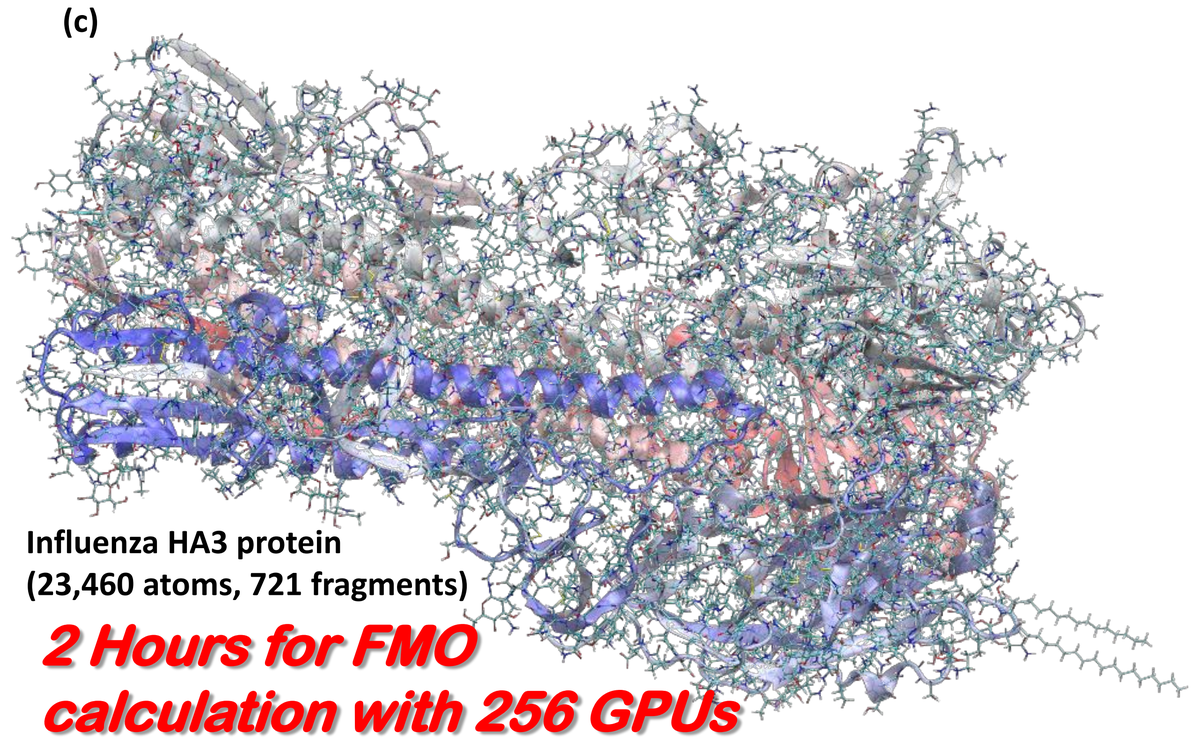

Fig. 1: (a) FMO calculation scheme, where large molecule is divided into many small fragments. Total molecular properties are reconstructed from the self consistent field (SCF) calculations of fragments and fragment-pairs with SCC (self-consistent-charge)-condition-satisfied electrostatic potential (ESP).
(b) Performance of GPU-accelerated FMO calculations. GPU-accelerated FMO-HF/6-31G(d) calculation of lysozyme with HA-PACS base cluster shows 3.8x speedups.
(c) As large-scale MO application, FMO-HF/6-31G(d) calculation of Influenza HA3 protein is successfully performed with 256 GPUs within two hours.

MD and QM/MM simulations using supercomputers

The world of life is full of mystery. Actual molecular structures, motions and chemical reactions of biological molecules, such as protein, nucleic acids, carbohydrates and lipids are still unclear. Using supercomputers, we have performed highly demanding computations based on molecular mechanics (MD) and hybrid quantum mechanics/molecular mechanics (QM/MM) methods, and we are uncovering some important biological questions.

(a)

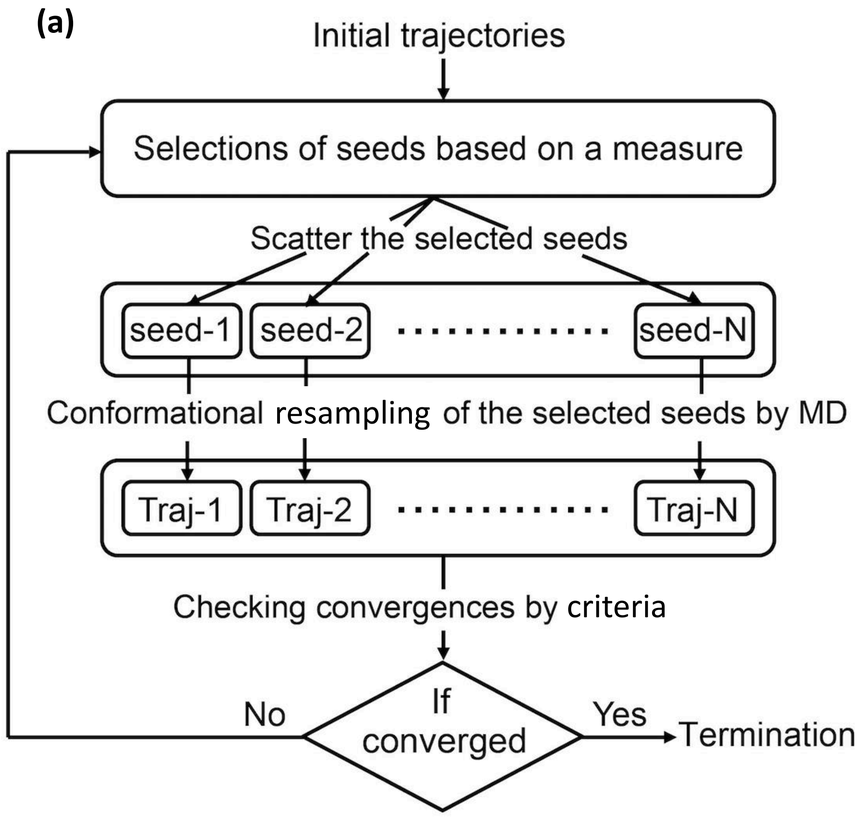

(b)

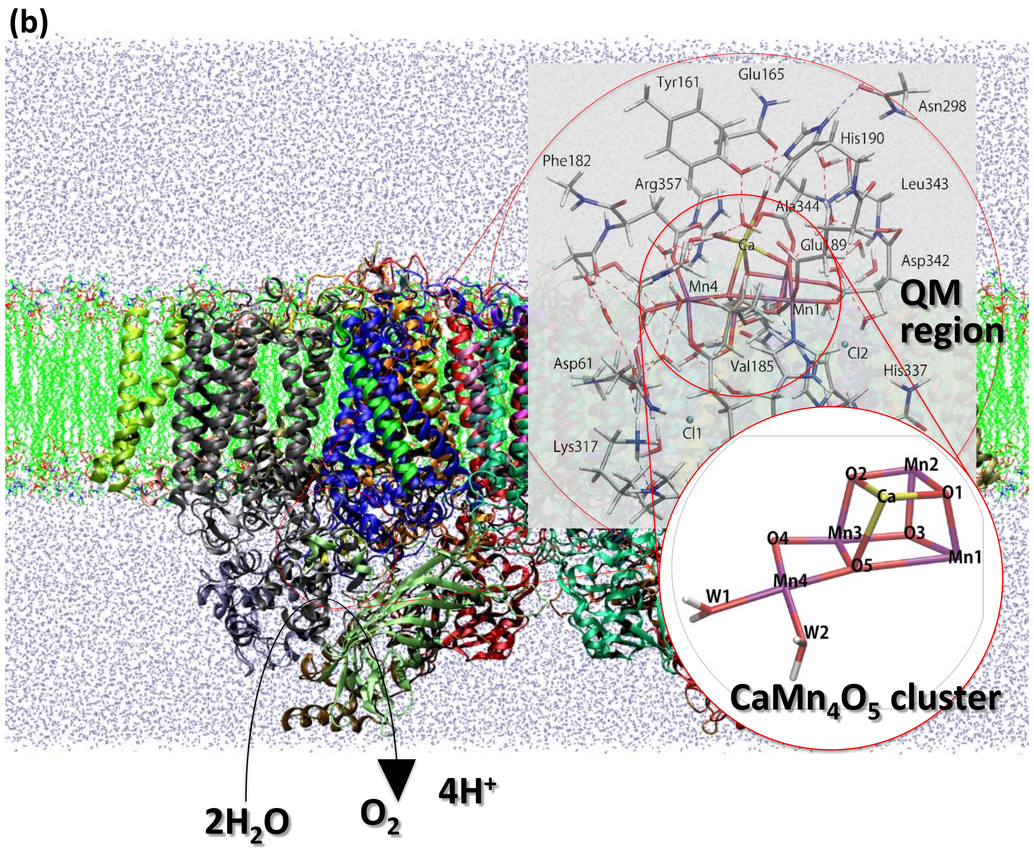

Fig. 2: (a) Effective conformational sampling of MD simulations: Parallel Cascade Selection MD (PaCS-MD). To promote the conformational transition, the following cycle is repeated in PaCS-MD; (I) Selections of initial seeds (structures) that have high potential to transit. (II) The conformational resampling through restarting multiple MD simulations from the selected initial seeds. [R. Harada et al., J. Chem. Phys. 139 035103 (2013)]
(b) QM/MM model of oxygen evolving complex in photosystem II. Key intermediate states in the catalytic reaction "$2H_2O$ + 4hv -> $4H^+$+$4e^-$ +O_2" have been investigated using the large model. [M. Shoji et al., Catal. Soc. Technol., 3, 1831 (2013).]

contact address: shigeta@ccs.tsukuba.ac.jp

Biological Sciences

338-gene analyses resolved the phylogenetic affiliation of a microeukaryote *Microheliella maris.*

Previously published phylogenetic studies failed to elucidate the phylogenetic position of a heliozoan microeukaryote *Microheliella maris*. Thus, we took a "phylogenomic" approach to place *M. maris* in the global tree of eukaryotes with accuracy. In the phylogeny inferred from an alignment containing 338 genes, *M. maris* branched at the base of the clade of a diverse collection of microeukaryote collectively called Cryptista with high statistical support.

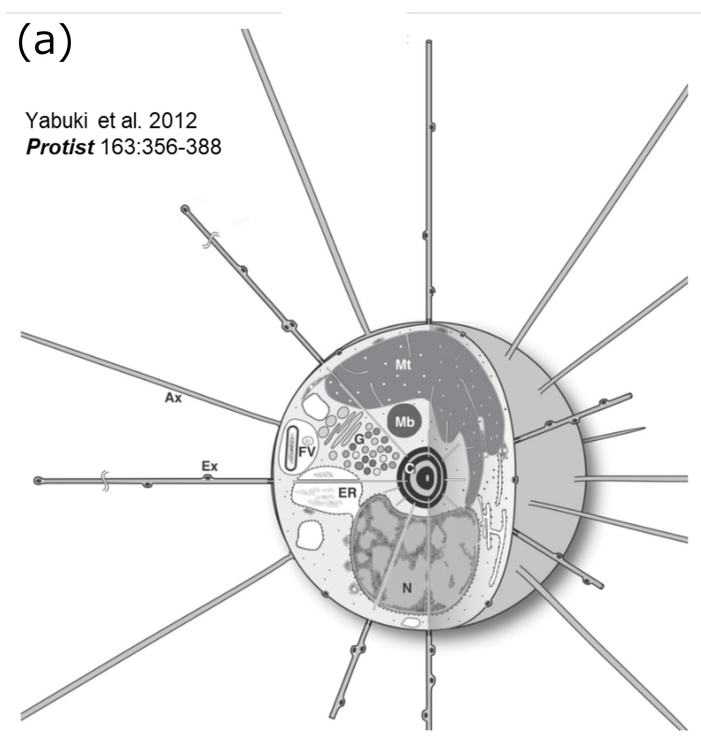

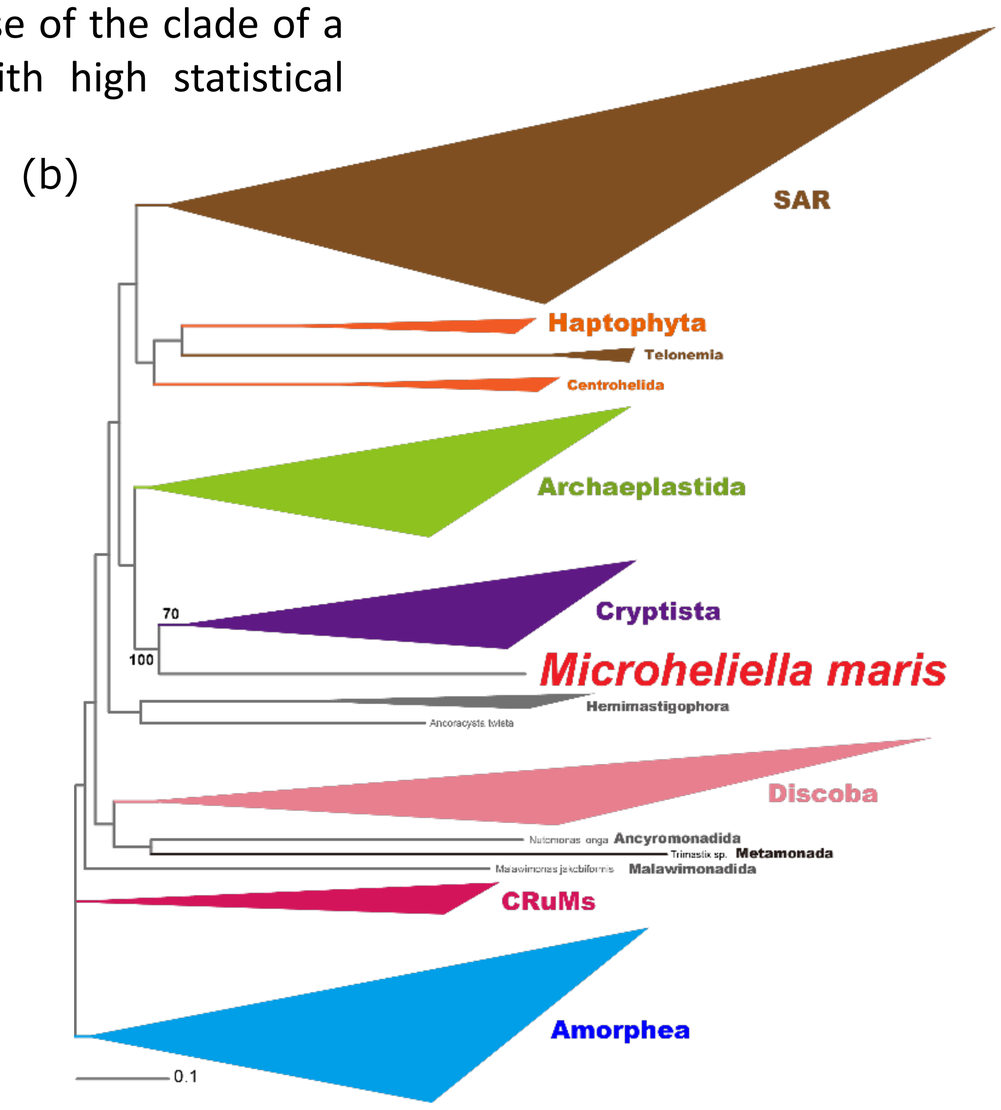

Fig. 1a: Schematic cell drawing of *Microheliell maris*.

Fig. 1b: Maximum likelihood phylogeny inferred from the 338-gene alignment.

In silico structural modeling and analysis of translation elongation factor 1α proteins

Translation elongation factor-1α (EF-1α) interacts with tRNA during protein synthesis. Some eukaryotes appeared to possess highly divergent EF-1α (^{div}EF-1α), implying that these proteins lack the ability to interact with tRNA. We modelled the tertiary structures of ^{div}EF-1α and validated their model structures by molecular dynamics simulations. We found that the molecular surfaces of ^{div}EF-1α are negatively charged partly, suggesting that they may not interact with negatively charged tRNA as strongly as the canonical EF-1α with the positively charged surfaces.

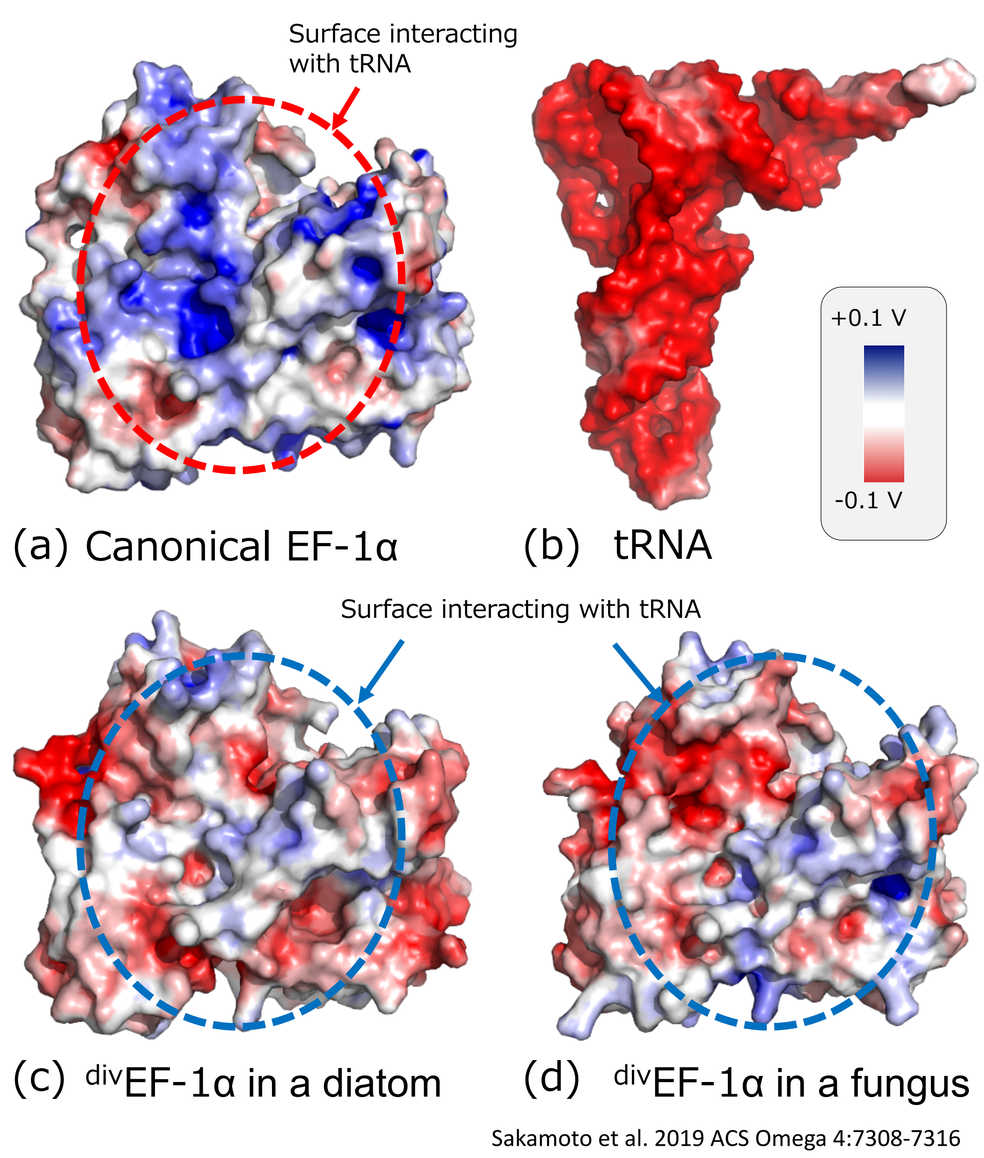

Fig. 2: EF-1α and tRNA structures and surface electrostatic distribution. (a) EF-1α structure of an archaeon (PDB ID: 3WXM). (b) tRNA structure (PDB ID: 1EHZ). (c & d) ^{div}EF-1α models. Dotted lines in (a), (c) and (d) indicate the surfaces interacting with tRNA.

Sakamoto et al. 2019 ACS Omega 4:7308-7316

contact address: yuji@ccs.tsukuba.ac.jp

Division of Global Environmental Sciences

Simulation of Atmospheric General Circulation by Global Cloud Resolving Model, NICAM

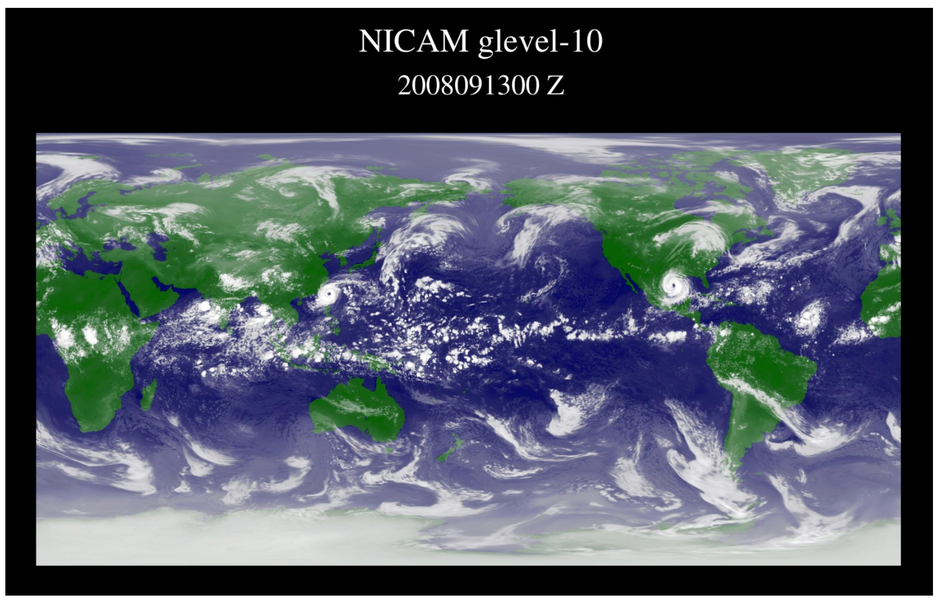

NICAM (Nonhydrostatic ICosahedoral Atmospheric Model) is able to reproduce the multi-scale cloud systems realistically, cumulus convection, Tropical cyclones, Arctic cyclones, the Madden–Julian Oscillation (MJO), and Intertropical Convergence Zone (ITCZ).

In Fig. 1, NICAM with glevel-10 (7-km horizontal resolution) well simulates Typhoon Shinraku near the Philippine Islands and Hurricane IKE near the Gulf of Mexico.

Fig. 1: Numerical simulation of the general circulation of the atmosphere produced by 7-km resolution NICAM.

Development of LES Model for thermal environment at city scale

Our group has been developing a Large Eddy Simulation (LES) model for urban environment. The main features of the model include (i) Building resolving, (ii) Roadside trees are resolved in vertical direction, (iii) Multiple reflections of short- and long-wave radiation between buildings and trees by radiosity method, (iv) resolving shadows from buildings and trees, and (v) incorporation of cloud physics and atmospheric radiation models. Numerical simulation of thermal environment around Tokyo station was conducted using Oakforest-PACS supercomputer. The total number of grid points is about 100 million.

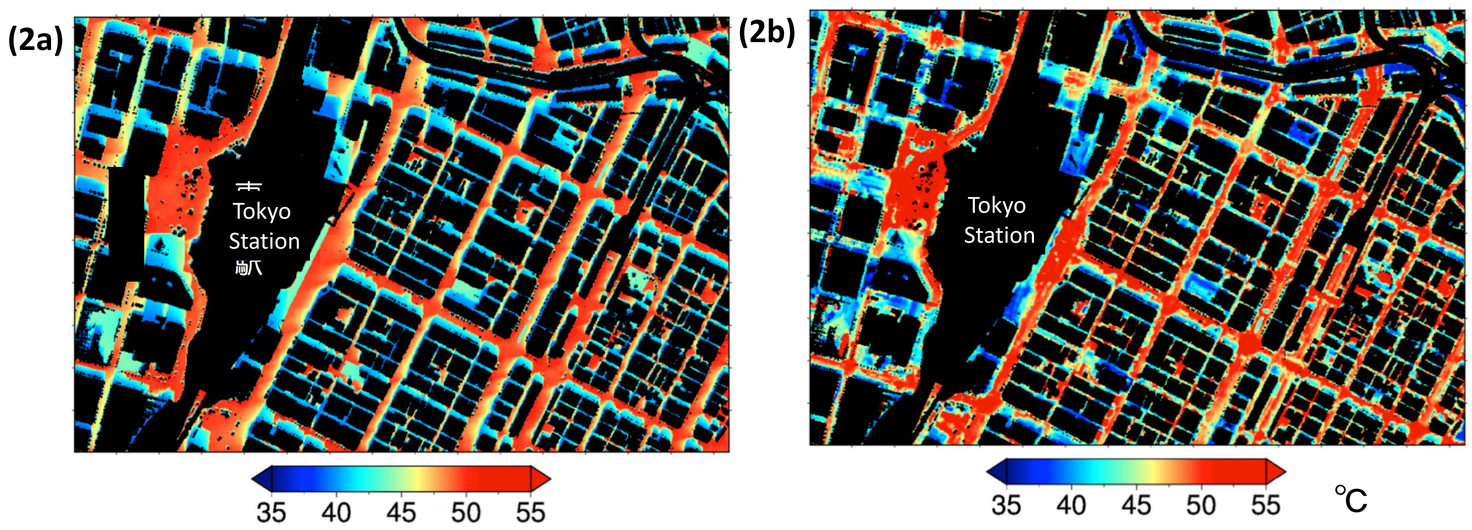

Fig. 2: Road skin temperature distribution estimated by the CCS-LES model (2a) and helicopter observation (2b). Black indicates buildings.

Hurricane forecast using an operational numerical weather prediction model

ECMWF OpenIFS

A easy-to-use version of Integrated Forecast Systems (IFS) operated at ECMWF (European Centre for Medium-range Weather Forecasts).

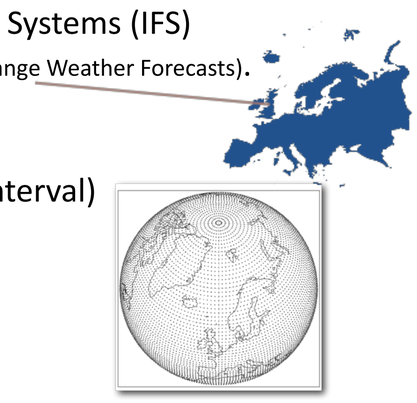

- Hydrostatic global spectral model (max resolution T1279: about 14km grid interval)
- Reduced Gaussian Grid
- Hybrid MPI-OpenMP scheme (Non-GPU, Non-FPGA)

Experimental settings

Version	cy40r1 (ECMWF, 2014) operational ver. in 19 Nov. 2013 - 11 May 2015
Initial condition	Atmosphere: GFS high-res analysis Land & Sea: ERA5 reanalysis
Model resolution	T639 L91 (32km grid spacing on the equator and 91 vertical levels)
Forecast length	240 hours (960 time steps with dt =900 s)
Computer	
Parallelisation	256 MPI procs (16 nodes * 16 procs/node) 4 OpenMP threads/process

Results - forecast of Hurricane Joaquin (2015) -

The experimental result showed a cyclone track similar to the NCEP control forecasts (thick line), suggesting that the initial conditions had a larger impact on the track forecast than NWP models in this case.

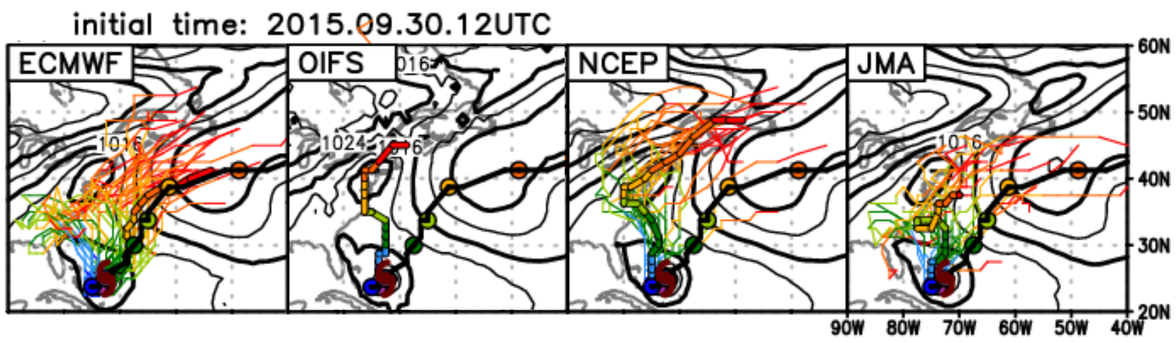

Fig. 3: Predicted cyclone tracks of Hurricane Joaquin (coloured lines) by ECMWF (Europe, left), the OpenIFS experiment (second left), NCEP (US, second right) and JMA (Japan, rightmost). Black lines shows observed track.

Remark

Computation time have decreased by 40% with Intel MKL Library in comparison with LAPACK.

Computation Time	3:12:38 (19 minutes for 1 day forecast)
Data size of output	9.9 GB

Database Group

Scalable Graph Analysis over Intel Xeon Phi Coprocessors

The structural graph clustering method *SCAN* is successfully used in many applications since it detects not only densely connected nodes as clusters but also extracts sparsely connected nodes as hubs or outliers (Fig. 1). However, it is difficult to apply SCAN to large-scale graphs since SCAN needs to evaluate the density for all adjacent nodes included in the graph. In this work, so as to address the above problem, we present a novel algorithm *SCAN-XP* that performs on Intel Xeon Phi coprocessors. We designed SCAN-XP to make the best use of many cores in the Intel Xeon Phi by employing the following approaches: First, SCAN-XP avoids the bottlenecks that arise from parallel graph computations by providing good load balances among the cores. Second, SCAN-XP effectively exploits 512 bit SIMD instructions implemented in each core to speed up the density evaluations. As a result, SCAN-XP runs approximately 100 times faster than SCAN; for the graphs with 100 million edges, SCAN-XP is able to perform in a few seconds (Fig. 2).

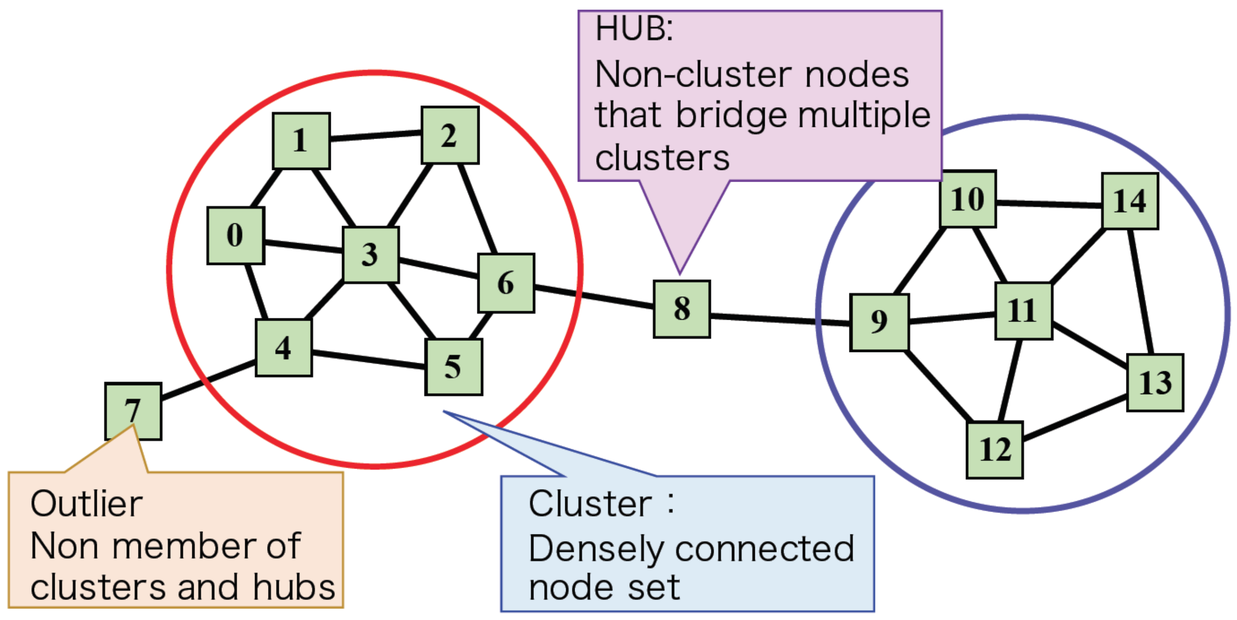

Fig. 1: Structural Graph Clustering SCAN

Table. 1: Real-world Dataset

Dataset	# of nodes	# of edges
com-youtube	1,134,890	2,987,624
web-BerkStan	685,230	6,649,470
soc-Pokec	1,632,803	22,301,964
com-LiveJournal	3,997,962	34,681,189
soc-LiveJournal1	4,846,609	42,851,237
com-Orkut	3,072,441	117,185,083
webbase2001	115,554,441	854,809,761

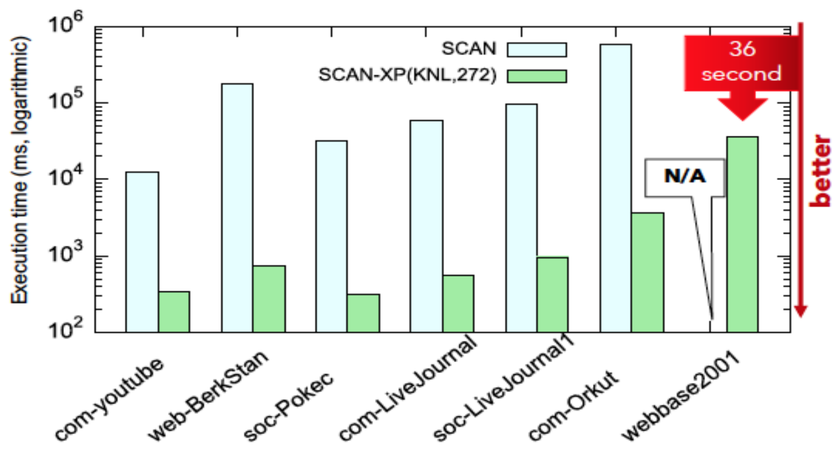

Fig. 2: Overall performances

Noise-robust sleep stage scoring for mice using deep learning & big data

Sleep stage scoring for mice is one of the most basic analyses in sleep research; however, this analysis is time-consuming and requires considerable expertise and effort. Although several studies have proposed automated scoring methods, they do not achieve robustness against noise in biological signals enough for research uses. To develop a noise-robust scoring method, we employ the following approaches.

1) Employing convolutional neural networks (CNN) & long short-term memory (LSTM), which can locate the feature of both biological signals and noise in them.
2) Training the model using noisy biological signals obtained from over 3000 mice.

Thank to these improvements, the proposed method achieved scoring accuracy of more than 95% for noisy biological signals. This result indicates that our method is practical enough for sleep research uses.

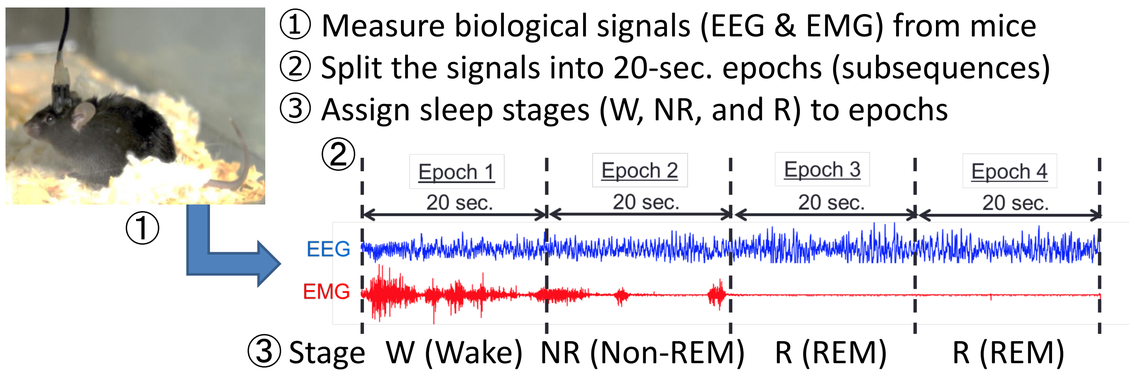

Fig. 3: Procedure of sleep stage scoring

Table 2: Feature of each stage

Stage	Peak Freq. of EEG	Amplitude of EMG
W	7-11 Hz	Large
NR	1-6 Hz	Small
R	7-11 Hz	Smallest

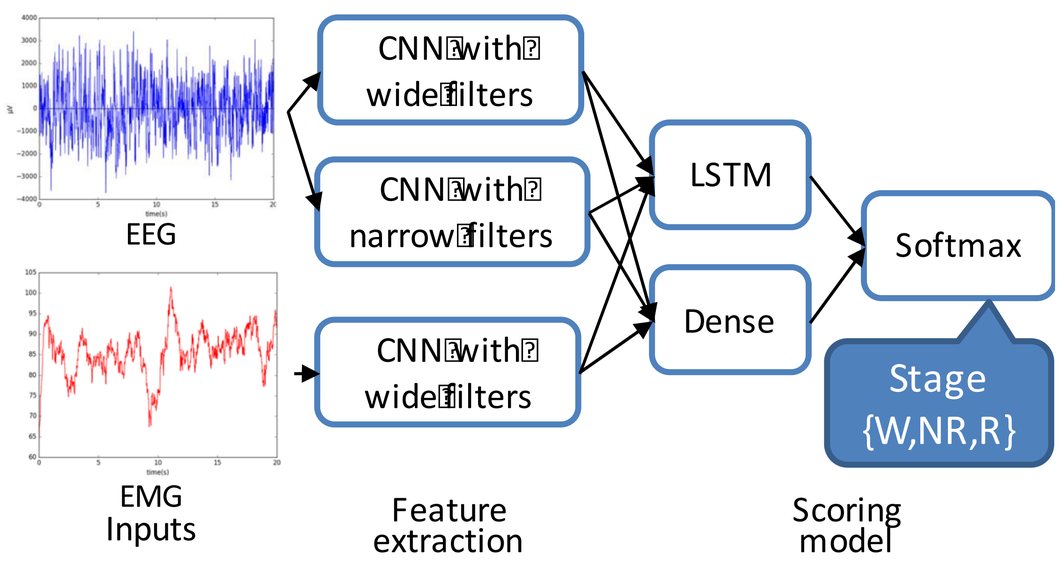

Fig. 4: Structure of the proposed system

contact address: {kitagawa, amagasa, shiokawa, horie}@cs.tsukuba.ac.jp

Computational Media Group

Information Display Design on Turn-By-Turn Navigation for Visually Impaired People

We are researching navigation for the visually impaired. We propose a new interface that utilizes sound and vibration to support turn-by-turn navigation that is common for visually impaired. In our proposed interface, the target path is divided into straight segments and points of change direction. The navigation instruction given by the sound and vibration is carefully designed to give minimum yet sufficient clues on the visually impaired walking. We have implemented a preliminary system based on our proposal and conducted a subject experiment for visually impaired people. The results imply that our proposed approach is useful for visually impaired navigation.

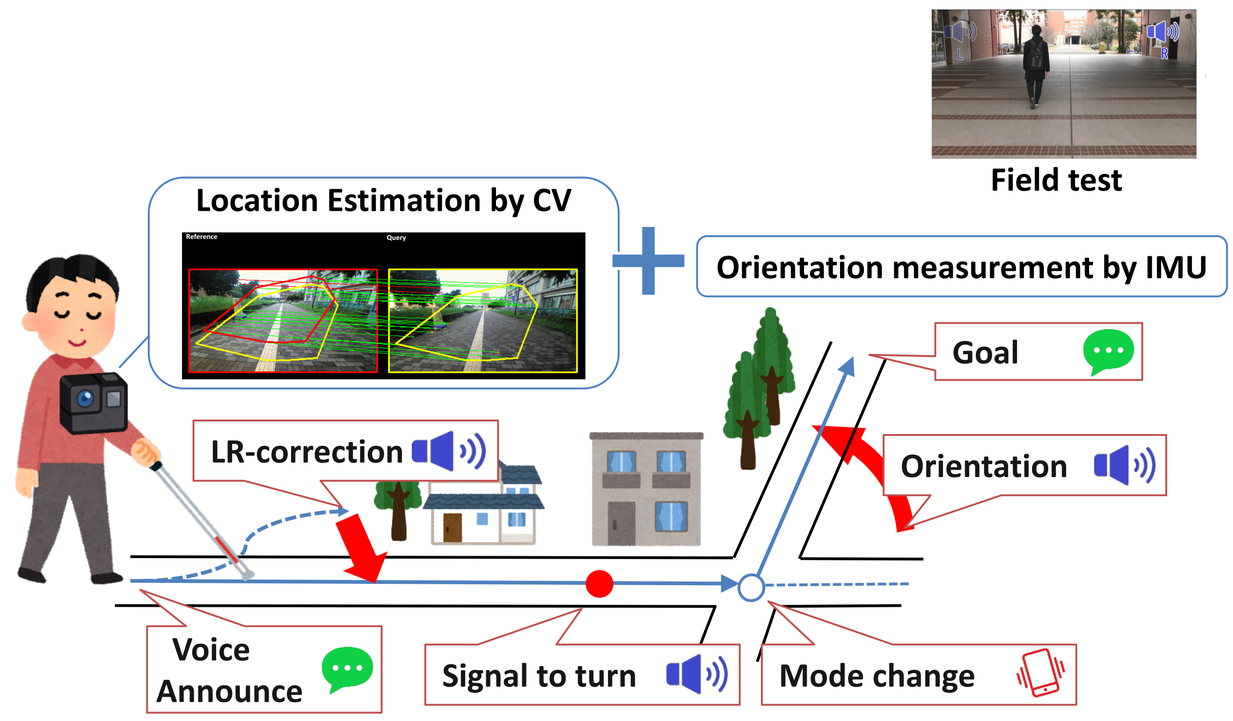

Image-quality Improvement of Omnidirectional: Free-Viewpoint Images by GAN

We proposes a method to improve the quality of omnidirectional free-viewpoint images using generative adversarial networks (GAN). By estimating the 3D information of the capturing space while integrating the omnidirectional images taken from multiple viewpoints, it is possible to generate an arbitrary omnidirectional appearance. However, the image quality of free-viewpoint images deteriorates due to artifacts caused by 3D estimation errors and occlusion. We solve this problem by using GAN and, moreover, by focusing on projective geometry during training, we further improve image quality by converting the omnidirectional image into perspective-projection images.

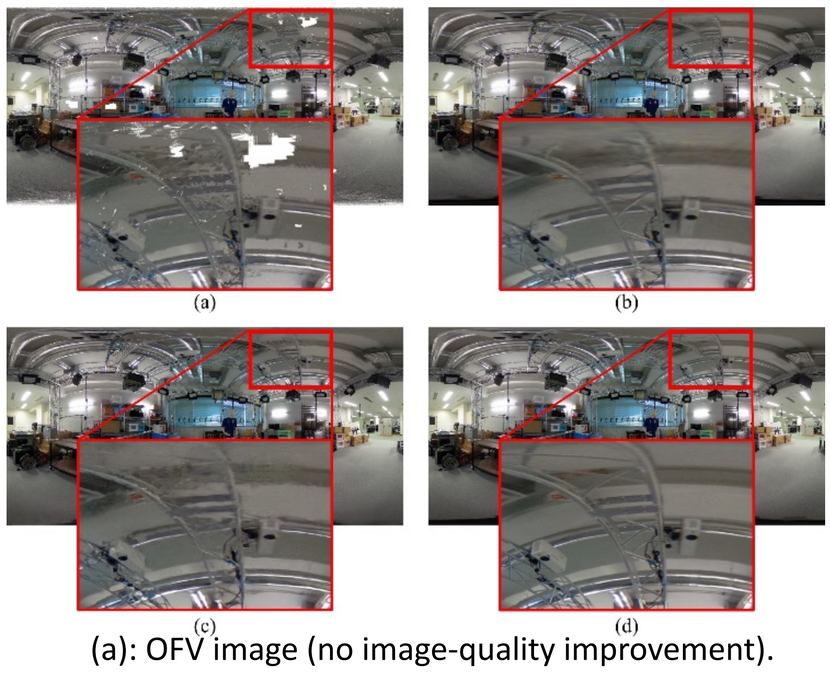

(a): OFV image (no image-quality improvement).
(d): Correct image (captured image).
(b): Proposed method using learning by image division (with image-quality improvement).
(c): Proposed method using learning with omnidirectional images (with image-quality improvement).

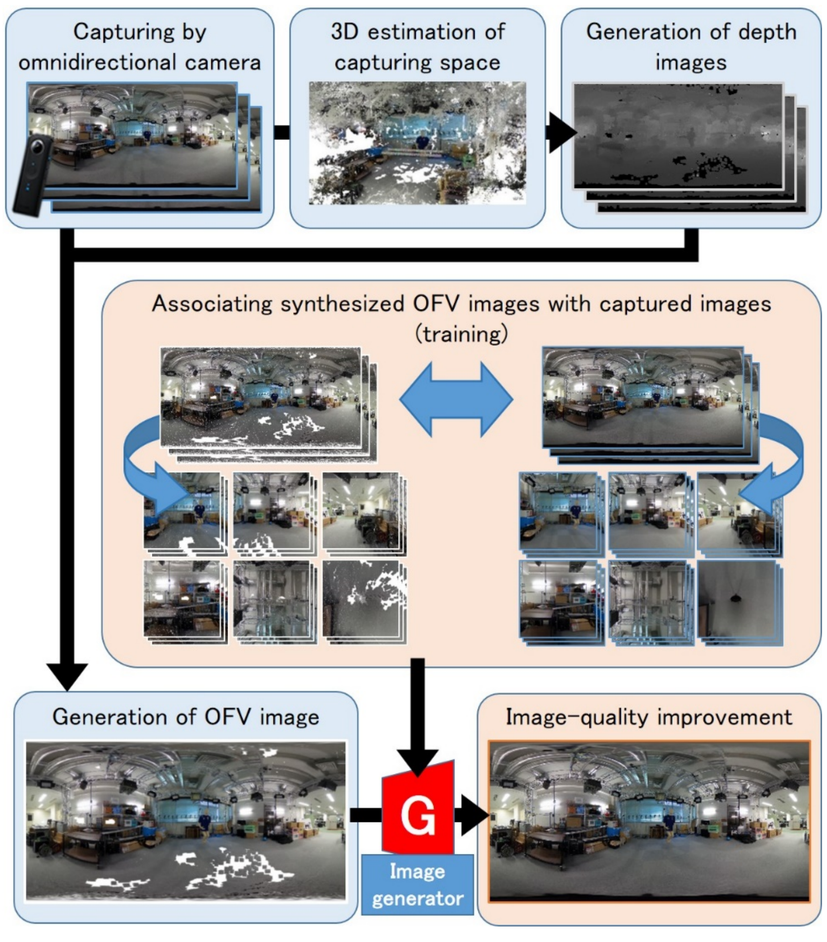

Accurate Overlapping Method of Time-Lapse Images for World Heritage Site Investigation

A method is proposed to accurately overlap multiple high-quality images with different shooting positions and intervals by combining corresponding point information between images and 3D shape information. In the proposed method, the correct feature matching of images obtained by rendering the 3D model of the subject is used. In this research, the subjects were the pillars of the Angkor Thom Bayon Temple and the epilithic microorganisms adhering to and eroding their surfaces. Synthetic transformation of a homography utilizing the correct matches is employed to overlap the target images.

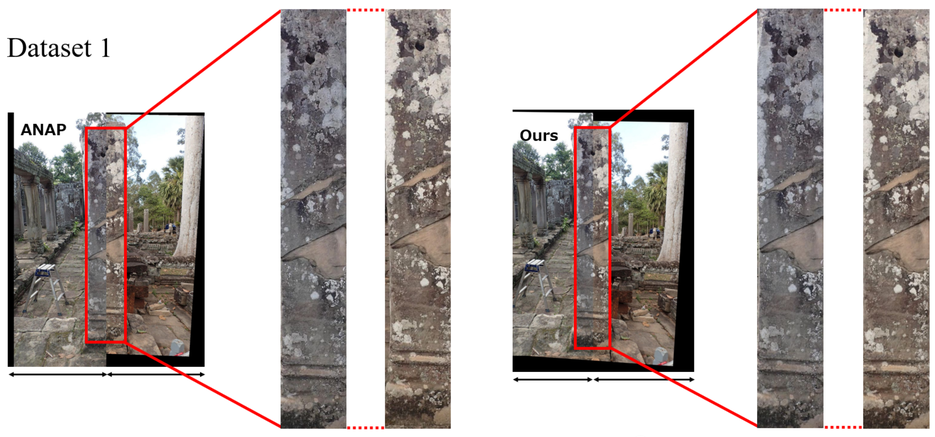

ANAP
PSNR：13.56
SSIM：0.07

Ours
PSNR：18.74
SSIM：0.64

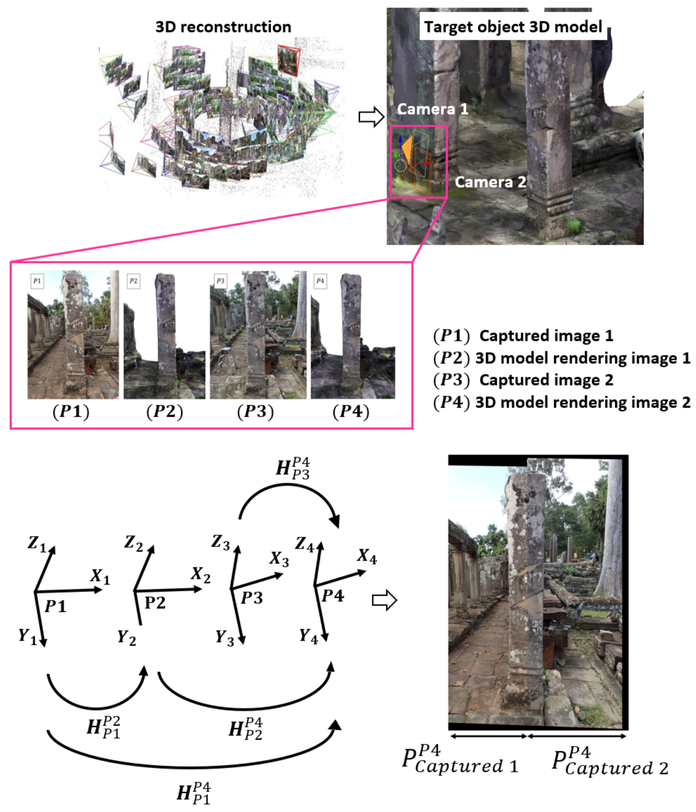

contact address: pr@ccs.tsukuba.ac.jp